JOURNAL OF COMPUTATIONAL PHYSICS **132,** 62–77 (1997)
ARTICLE NO. CP965609

Numerical Algorithms for Flows in the Nodes of 2D Models of Pipe Networks

Vladimir Karlin

The Robert Gordon University, Schoolhill, Aberdeen AB10 1FR, United Kingdom

Received January 8, 1996; revised October 28, 1996

This work is aimed at developing efficient computational algorithms for numerical simulation of steady-state incompressible viscous flows in nodes of circulation networks. High order accuracy implicit stabilization algorithms based on upwind finite-difference schemes were proposed. In order to treat complicated geometry, decomposition of computational domains was used. The effect of an external circulation network was simulated by means of nonlocal boundary conditions linking inlet and outlet flow parameters. A fluid flow related to specific cardiovascular operation was studied numerically as an example.

1. INTRODUCTION

Flows in complex nodes of pipe networks are often encountered in a wide area of modern engineering applications and should be carefully investigated in order to optimize the related technological processes. Unlike a number of detailed tables devoted to fluid flows in pipe junctions, there are some problems which are still sparingly represented. For example, the fundamental handbook of hydraulic resistance [8] provides a huge array of empirical data, mostly for turbulent flow regimes, but it does not contain adequate information on flow patterns. However, resistances to laminar flows and the corresponding vortex structures are also of interest for engineering applications. Additionally, in some cases a pipe junction has to be considered as part of a specific circulation network with essential mutual interaction. Cardiovascular and assisted circulation systems may serve as examples of such networks.

At present, numerical modelling of cardiovascular fluid dynamics is undertaken in two main directions. The first one is based on multidimensional Navier–Stokes models of flows in specific parts of the circulation system. For example, flows in bifurcating arteries were studied numerically in [7], where further references can be found. Numerical model of 3D time-dependent fluid flow in an artificial heart was developed and investigated in [10], and, finally, a realistic numerical model of human heart was elaborated and reported in [14]. These Navier–Stokes (or ''differential'') models provide detailed data about local flow structure but do not take into account a feedback of the flow in the considered computational region on the rest of the circulation network. In contrast, hydraulic one-dimensional (or ''integral'') models of the whole cardiovascular circulation network take into account the mutual interaction of all components of the network, but they are incapable of providing any data on the fluid flow structure, except the distribution of averaged pressure and mass flow rate along the network (see, for example, [19]).

In this work an attempt to combine a global hydraulic model of a circulation network with a detailed Navier–Stokes simulation of flow in a pipe junction was undertaken. In order to attain the aim, we proposed using one-dimensional hydraulic models as the inlet/outlet boundary conditions in Navier–Stokes models of flows in pipe junctions.

Configurations of considered pipe junctions are depicted in Figs. 1.1 and 1.2. We call them T- and X-geometry, respectively, and suppose that the T-geometry is part of a simple circulation system shown in the right of Fig. 1.1, while X-geometry corresponds to some complicated circulation system illustrated in the right of Fig. 1.2.

Fluid flow in the X-geometry is related to a surgical treatment of cardiovascular systems which is known as the total cavopulmonary anastomosis [5, 15]. It is used to treat congenital anomalies of the right side of the heart and consists of, in particular, an artificial junction between the superior vena cava and the right pulmonary artery. The right side of the heart is almost excluded from the circulation. The cavopulmonary junction should be made to maximize the circulation rate. On the other hand, it should not lead to extra-mechanical hemolysis. There are three parameters to optimize in the model depicted in Fig. 1.2: i.e., the inclination angles α_ν, $\nu = 1, 2$, and displacement Δl between the inlet branch pipes. Figure 1.3 illustrates the operation of the total cavopulmonary anastomosis.

Numerical algorithms used in this work are built on the basis of up to the fifth-order upwind finite-difference schemes for the Navier–Stokes equations [17]. Such an approach has been proven to be efficient for both incompressible [17] and compressible [21] viscous flows. In absence of boundary layers these upwind high order approxi-

0021-9991/97 $25.00

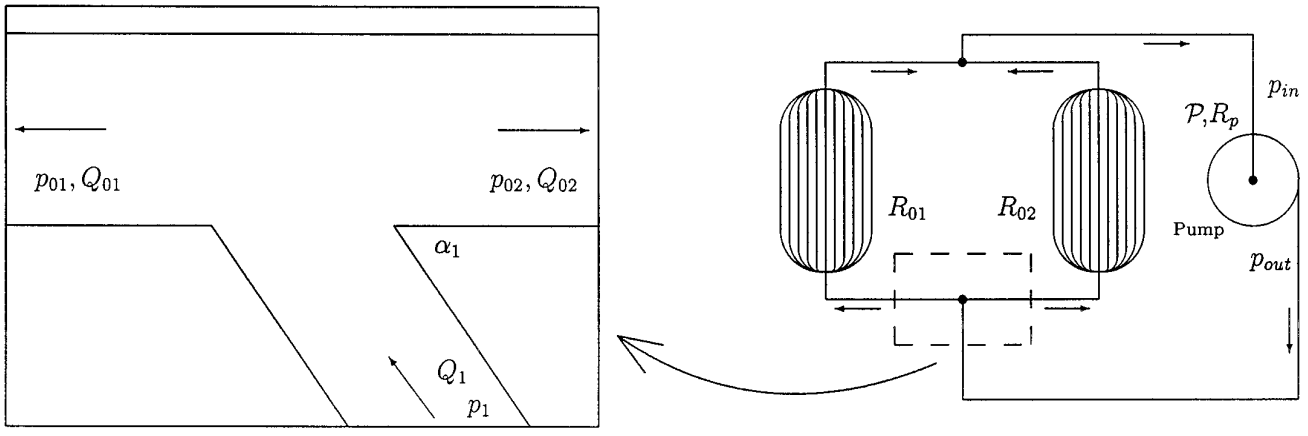

FIG. 1.1. *T*-junction in a simple circulation system.

mations are reasonably accurate, even on sparse numerical grids, and may be used to analyze sizable parts of circulation networks efficiently.

Geometrical complexity of the considered computational domains renders it inefficient to use a global boundary-fitted curvilinear grid. In order to overcome this difficulty, the computational domain was decomposed into a number of relatively simple overlapping subdomains where affine equidistant grids were used. These simple grids are quite advantageous for the problem in question, as laminar flows in pipes are usually free of boundary layers and, on the other hand, their use reduces the computer resources required for computation of the coefficients of finite-difference schemes. Also, the interpolation procedure in the overlapping area, which is crucial for achieving the overall high accuracy [3], is much simpler and accurate for affine equidistant grids.

A kind of ADI factorization was employed to discretize the problem in time. This approach gives rather stable numerical algorithms for multidimensional problems and

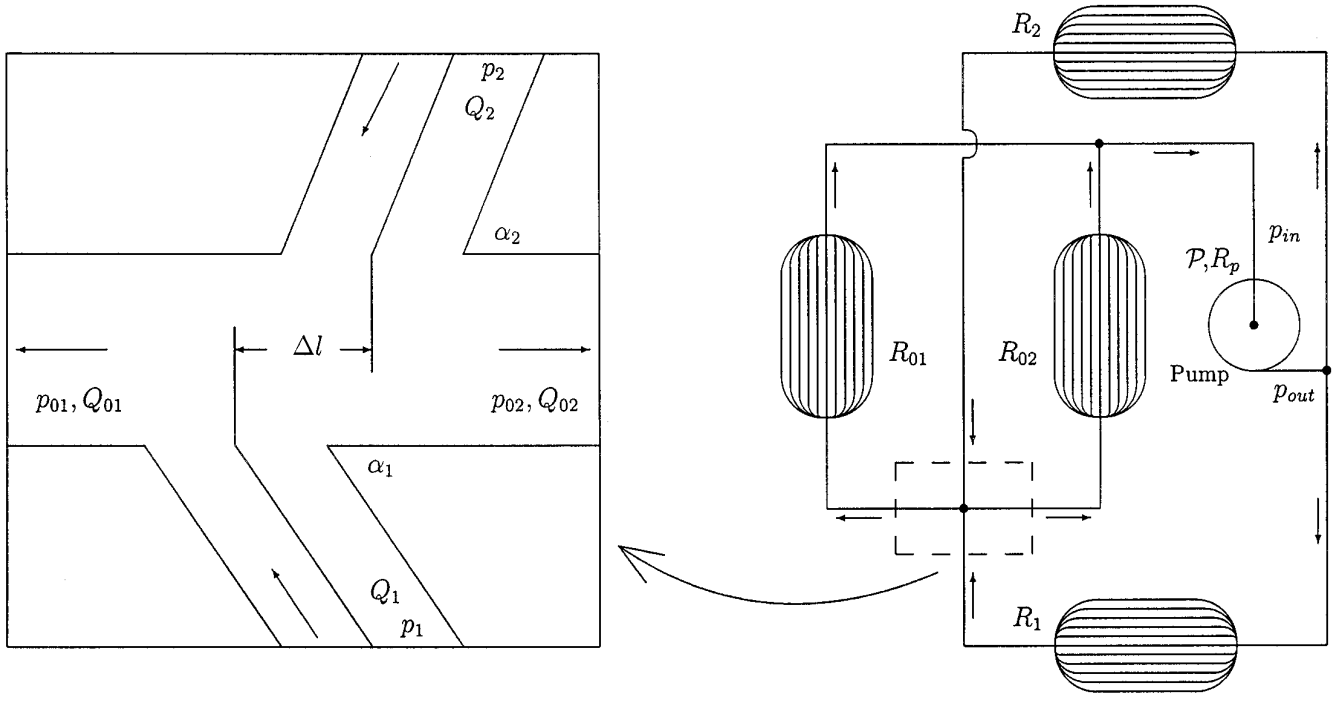

FIG. 1.2. *X*-junction in a complicated circulation system.

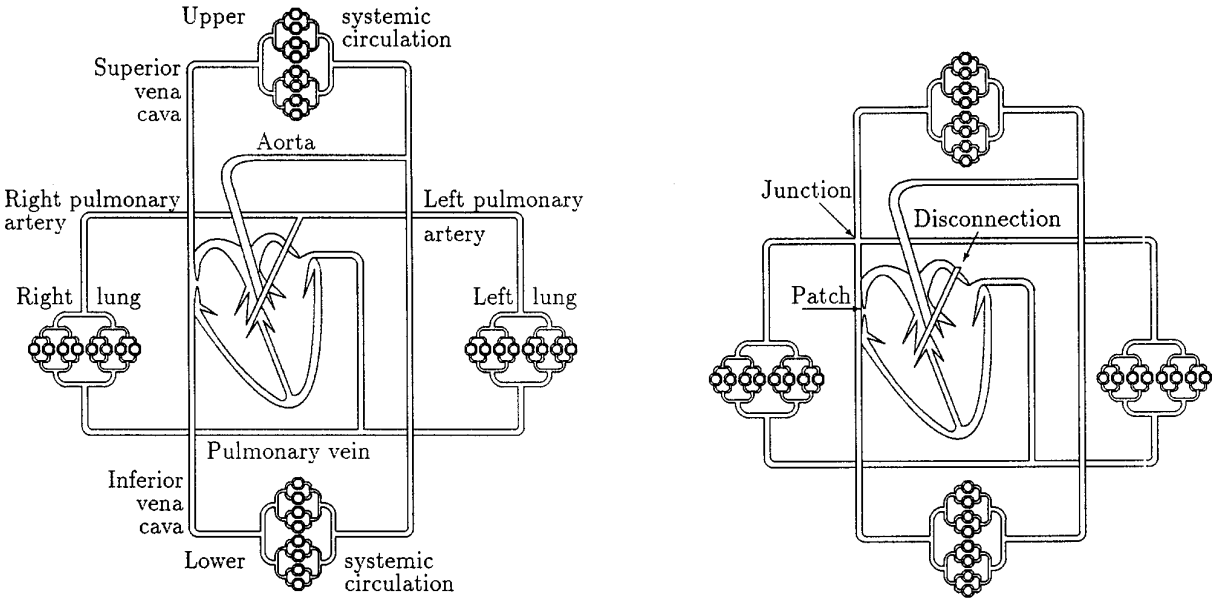

FIG. 1.3. Cardiovascular system before (left) and after (right) surgical treatment.

provides certain opportunities for parallelization. In particular, it is quite efficient for Navier–Stokes computations [13].

2. GOVERNING EQUATIONS AND BOUNDARY CONDITIONS

The geometry of the whole computational domain provides a natural path for splitting into two or three parallelograms, as shown in Fig. 2.1. Ortholinear coordinates (x_0, y_0) with the origin as the geometrical center were used in D_0. The coordinates in the inlet branch pipes were obtained from (x_0, y_0) by applying the affine transform

$$x_\nu = x_0 - \left[(-1)^\nu y_0 - \frac{d_0}{2}\right]\cot\alpha_\nu - (-1)^\nu \frac{\Delta l}{2},$$
$$y_\nu = (-1)^\nu y_0 - \frac{d_0}{2}, \quad \nu = 1, 2, \tag{2.1}$$

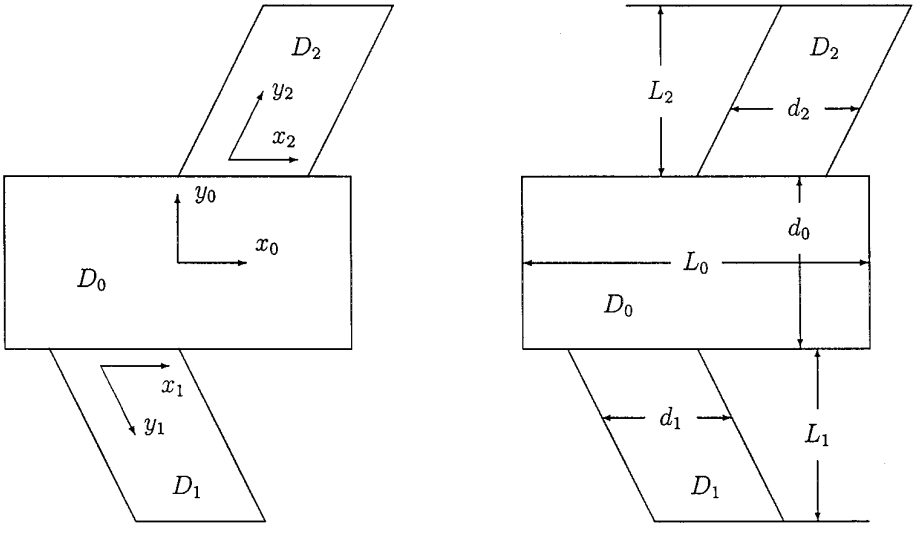

FIG. 2.1. Computational domains and coordinate systems.

depending on the inclination angle α_ν. The diameter d_0 of the central collecting pipe D_0 was used as the unit length in this work.

Fluid flows which are governed by the Navier–Stokes equations for primitive variables were considered. In order to treat the steady-state flows, a variant of an artificial compressibility method [4] was employed,

$$A_t \frac{\partial U}{\partial t} + \frac{\partial W_{x,\nu}}{\partial x_\nu} + \frac{\partial W_{y,\nu}}{\partial y_\nu} = \mathrm{Re}^{-1} B \left[(1 + \cot^2\alpha_\nu) \frac{\partial^2 U}{\partial x_\nu^2} - 2 \cot\alpha_\nu \frac{\partial^2 U}{\partial x_\nu \partial y_\nu} + \frac{\partial^2 U}{\partial y_\nu^2} \right],$$
$$(x_\nu, y_\nu) \in D_\nu, \quad t > 0, \quad \nu = 0, 1, 2, \tag{2.2}$$

where

$$U = (p, v_x, v_y)^{\mathrm{T}}, \quad A_t = \mathrm{diag}(\beta_p, \beta_x, \beta_y),$$
$$B = \mathrm{diag}(0, 1, 1), \quad \alpha_0 = \frac{\pi}{2}, \tag{2.3}$$

$$W_{x,\nu} = \begin{pmatrix} \beta v_x - (-1)^\nu \beta v_y \cot\alpha_\nu \\ p + v_x^2 - (-1)^\nu v_x v_y \cot\alpha_\nu \\ v_x v_y - (-1)^\nu \cot\alpha_\nu (p + v_y^2) \end{pmatrix},$$
$$W_{y,\nu} = (-1)^\nu \begin{pmatrix} \beta v_y \\ v_x v_y \\ p + v_y^2 \end{pmatrix}, \tag{2.4}$$

and the usual notations for pressure $p(t, x_\nu, y_\nu)$, velocity components $v_x(t, x_\nu, y_\nu)$, $v_y(t, x_\nu, y_\nu)$ in ortholinear coordinates x_0, y_0, and the Reynolds number Re were used. Equations (2.2)–(2.4) reduce to the Navier–Stokes system if parameters of artificial compressibility are assigned the following values: $\beta_p = 0$ and $\beta = \beta_x = \beta_y = 1$.

As usual, a constraint upon solutions to the system (2.2)–(2.4) that the velocity of the flow vanishes at the solid walls have been posed. Neither pressure nor mass flow rate are given at the inlet/outlet boundaries of the domain $D = D_0 \cup D_1 \cup D_2$. These factors depend on the rest of the network and have to be defined in the numerical experiment. Some special consideration is required in order to evaluate the proper inlet/outlet boundary conditions.

Let us consider a problem

$$A_t \frac{\partial U}{\partial t} + A_{x,0} \frac{\partial U}{\partial x_0} = 0, \quad x_0 > 0, \quad t > 0 \tag{2.5}$$

with

$$A_{x,0} = \frac{\partial W_{x,0}}{\partial U} = \begin{pmatrix} 0 & \beta & 0 \\ 1 & 2v_x & 0 \\ 0 & v_y & v_x \end{pmatrix}$$

and explain what boundary conditions are acceptable at $x_0 = 0$. System (2.5) is hyperbolic, it models the dynamics of small disturbances of system (2.2) propagating along the coordinate direction $y_0 = \text{const}$. Vectors $N_1 = (1, -\beta_y v_x^{-1})^{\mathrm{T}}$ and $N_{2,3} = (\beta\beta_p^{-1}, v_x \pm \sqrt{v_x^2 + \beta\beta_x\beta_p^{-1}})^{\mathrm{T}}$ are normal to its characteristics. Coefficients of the corresponding characteristic relations are nontrivial solutions of the equations $\omega(N_{k,1}A_t + N_{k,2}A_{x,0}) = 0$, $k = 1, 2, 3$, and may be written in the form: $\omega_1 = (v_y[\beta_p\beta_y^{-2}v_x^2(\beta_x - 2\beta_y) - \beta]^{-1}, v_y[\beta_y^{-1}v_x(\beta_x - 2\beta_y) - \beta\beta_y\beta_p^{-1}v_x^{-1}]^{-1}, 1)$, $\omega_{2,3} = (v_x \pm \sqrt{v_x^2 + \beta\beta_x\beta_p^{-1}}, -\beta, 0)$. For the positive streamwise velocity component $v_x(t, 0) > 0$, vectors N_1 and N_3 are orthogonal to incoming characteristics and the corresponding sets of characteristic coefficients ω_1 and ω_3 show that some linear combinations of p, v_x, v_y and p, v_x should be specified at the inlet boundary. In the same manner, we conclude that only a linear combination of p and the streamwise velocity component v_x, corresponding to ω_3, should be specified at the outlet boundary, where streamwise velocity is negative, $v_x(t, 0) < 0$. It is important to note that ω_1 becomes simply (0, 0, 1) for the vanishing cross-flow velocity component v_y. Therefore, if the inlet cross-flow velocity component v_y is expected to be negligible, then it is expedient to specify it at that point.

Besides certain requirements arising from the well-posedness, the flow in question should be compatible with the rest of the network. ''Integral'' models of hydraulic networks are based on the conservation of mass and on a given dependence of the pressure drop upon the mass flow rate [9]. In this research we have restricted ourselves by a linear dependence, which is a good approximation for the human circulation system [2]. Then, the simplest network shown in Fig. 1.1 can be modelled by the formulas

$$p_1 = p_{\mathrm{out}},$$
$$p_{0\nu} = p_{\mathrm{out}} - \mathscr{P} + R_p(Q_{01} + Q_{02}) + R_{0\nu}Q_{0\nu}, \quad \nu = 1, 2, \tag{2.6}$$

and a complicated version as featured in Fig. 1.2 may be described in the form

$$p_{0\nu} = p_{\mathrm{out}} - \mathscr{P} + R_p(Q_{01} + Q_{02}) + R_{0\nu}Q_{0\nu},$$
$$p_\nu = p_{\mathrm{out}} - R_\nu Q_\nu, \quad \nu = 1, 2. \tag{2.7}$$

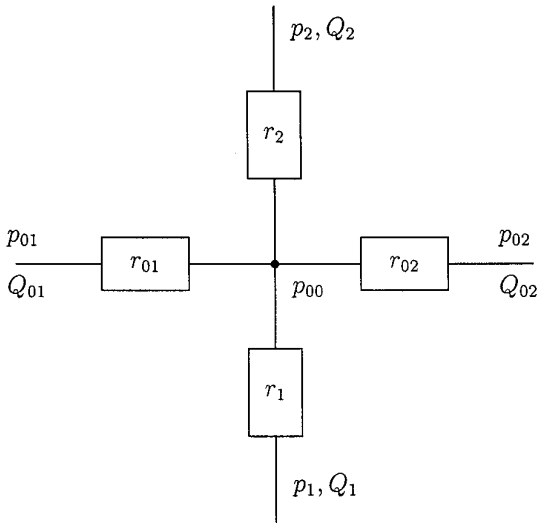

FIG. 2.2. An ''integral'' model of X-junction.

Here Q and R are mass flow rate and hydraulic resistance, respectively. Values of R_p, $R_{0\nu}$, R_ν and $\mathscr{P}$, p_{out} were considered as known parameters of the network and pump. Formulas (2.6), (2.7) assume that the pump works in a rated regime and is described by a linear equation $p_{\text{out}} - p_{\text{in}} = \mathscr{P} - R_p(Q_{01} + Q_{02})$.

Mass conservation relations $Q_1 = Q_{01} + Q_{02}$ and $Q_1 + Q_2 = Q_{01} + Q_{02}$ were not added to (2.6) and (2.7), respectively, because they are included in the ''differential'' flow model implicitly as a constituent part of (2.2)–(2.4). The following argument may serve as an explanation for completeness of the system (2.2)–(2.4) and (2.6) or (2.7). Let us consider an ''integral'' approximation to the flow in the X-configuration, for example the one depicted in Fig. 2.2. It is represented by the system

$$p_\nu - p_{00} = r_\nu Q_\nu, \quad p_{00} - p_{0\nu} = r_{0\nu} Q_{0\nu}, \quad \nu = 1, 2, \tag{2.8}$$

$$Q_1 + Q_2 = Q_{01} + Q_{02}. \tag{2.9}$$

The determinant of the system composed of (2.7), (2.8), and (2.9) equals

$$\begin{aligned}\delta = {} & (R_1 + r_1)(R_2 + r_2)(R_{01} + R_{02} + r_{01} + r_{02}) \\ & + (R_{01} + r_{01})(R_{02} + r_{02})(R_1 + R_2 + r_1 + r_2) \\ & + R_p(R_1 + R_2 + r_1 + r_2)(R_{01} + R_{02} + r_{01} + r_{02})\end{aligned}$$

and does not vanish if the network is not degenerated. Therefore, the coupled system may be uniquely resolved with respect to $Q_{0\nu}$, Q_ν, $p_{0\nu}$, Q_ν, and p_{00} for given $R_{0\nu}$, R_ν, $r_{0\nu}$, r_ν, and $\mathscr{P}$.

In realistic computations, some violation of mass conservation due to truncation or round-off errors is possible and Eq. (2.9) has to be changed to

$$Q_u + Q_d = Q_l + Q_r + \varepsilon, \tag{2.10}$$

where ε is a small number. The coupled system (2.7), (2.8), and (2.10) is still uniquely resolvable but its solution will depend on ε. For instance,

$$\begin{aligned}Q_1 = {} & \delta^{-1}(R_2 + r_2)\{(R_{01} + R_{02} + r_{01} + r_{02})\mathscr{P} \\ & - \varepsilon[(R_{01} + r_{01})(R_{02} + r_{02}) + R_p(R_{01} + R_{02} + r_{01} + r_{02})]\}\end{aligned}$$

shows that a tiny leakage of mass in the ''differential'' model will lead to a variation of the mass flow rate of the same order.

More complicated ''integral'' models of the X-junction would give more complicated, but still uniquely resolvable, systems. Therefore, relations like (2.9) were not used explicitly and any regulation of proportion of $Q_1/(Q_{01} + Q_{02})$ were not undertaken, assuming that it should appear in the steady-state solution automatically, once a well-posed initial boundary-value problem for (2.2)–(2.4) subjected to conditions of consistency (2.6) or (2.7) is solved. Moreover, the discrepancy between $Q_{01} + Q_{02}$ and $Q_1 + Q_2$ may serve as a measure of accuracy of computed solutions.

Specifically, a parabolic velocity profile with an unknown maximum was assumed at the inlet to the node. Together with conditions of consistency (2.7) it gives

$$\begin{aligned}v_x(t, x_\nu, L_\nu) &= v(t, x_\nu)\cos\alpha_\nu, \\ v_y(t, x_\nu, L_\nu) &= v(t, x_\nu)\sin\alpha_\nu,\end{aligned} \tag{2.11}$$

where

$$v(t, x_\nu) = \frac{6}{R_\nu d_\nu^3}\left(\frac{d_\nu^2}{4} - x_\nu^2\right)\left[p_{\text{out}} - d_\nu^{-1}\int_{-d_\nu/2}^{d_\nu/2} p(t, \xi, L_\nu)\, d\xi\right], \quad \nu = 1, 2.$$

At the outlet boundaries in the central collecting pipe a zero value of the cross-flow pressure gradient was specified, resulting in

$$\begin{aligned}p(t, (-1)^\nu L_0/2, y) = {} & p_{\text{out}} - \mathscr{P} + R_p \\ & \int_{-d_0/2}^{d_0/2}[v_x(t, L_0/2, \xi) - v_x(t, -L_0/2, \xi)]\, d\xi \\ & + (-1)^\nu R_{0\nu}\int_{-d_0/2}^{d_0/2} v_x(t, (-1)^\nu L_0/2, \xi)\, d\xi, \quad \nu = 1, 2,\end{aligned} \tag{2.12}$$

if combined with the conditions of consistency (2.7).

As an alternative to (2.11) an assumption of zero cross-flow velocity and pressure gradient may serve:

$$v_x = v_y \cot \alpha_\nu, \quad 2\frac{\partial p}{\partial x_\nu} = \frac{\partial p}{\partial y_\nu} \sin 2\alpha_\nu, \quad \nu = 1, 2. \tag{2.13}$$

In the chosen coordinate system the cross-flow direction coincides with the coordinate lines $y_\nu = \text{const}$ only if $\alpha_\nu = \pi/2$, such that an averaged value of p should be used in conditions of consistency (2.6) or (2.7),

$$d_\nu^{-1} \int_{-d_\nu/2}^{d_\nu/2} p(t, \xi, L_\nu)\, d\xi = p_{\text{out}} + R_\nu \int_{-d_\nu/2}^{d_\nu/2} v_y(t, \xi, L_\nu)\, d\xi, \quad \nu = 1, 2, \tag{2.14}$$

which are attached to (2.13).

Similarly, a parabolic stream-wise velocity law with an unknown maximum $v_{0\nu,\max}$ may be posed at the outlets:

$$v_x\left(t, (-1)^\nu \frac{L_0}{2}, y_0\right) = (-1)^\nu v_{0\nu,\max}\left(\frac{d_0^2}{4} - y_0^2\right), \quad \nu = 1, 2.$$

Then, it may be transformed to the relations

$$\begin{aligned} &R_p[v_x(t, L_0/2, y_0) - v_x(t, -L_0/2, y_0)] \\ &\quad + (-1)^\nu R_{0\nu} v_x(t, (-1)^\nu L_0/2, y_0) = \frac{6}{d_0^3}\left(\frac{d_0^2}{4} - y_0^2\right) \\ &\quad \left[d_0^{-1} \int_{-d_\nu/2}^{d_\nu/2} p(t, (-1)^\nu L_0/2, \xi)\, d\xi - p_{\text{out}} + \mathscr{P}\right], \quad \nu = 1, 2, \end{aligned} \tag{2.15}$$

by taking into account conditions of consistency (2.6) or (2.7).

Eventually, we suppose that some initial conditions at $t = 0$,

$$U(0, x_\nu, y_\nu) = U^{(0)}(x_\nu, y_\nu), \quad (x_\nu, y_\nu) \in D_\nu, \quad \nu = 0, 1, 2, \tag{2.16}$$

are given for the system (2.2)–(2.4).

The arguments developed in this section are only heuristic and may not serve as a formal base for evaluation of proper inflow/outflow boundary conditions. However, experience shows that they generate well-posed problems and plausible results in rather complicated flow situations.

3. NUMERICAL ALGORITHM

Equidistant numerical grids which may be represented in the following form were used in this work,

$$\begin{aligned} &x_{0,i} = ih_{x,0}, \ i = -N_{x,0}, ..., N_{x,0}, \quad h_{x,0} = L_0/2N_{x,0}, \\ &y_{0,j} = jh_{y,0}, \ j = -N_{y,0}, ..., N_{y,0}, \quad h_{y,0} = d_0/2N_{y,0}, \\ &x_{\nu,i} = ih_{x,\nu}, \ i = -N_{x,\nu}, ..., N_{x,\nu}, \quad h_{x,\nu} = d_\nu/2N_{x,\nu}, \quad \nu = 1, 2, \\ &y_{\nu,j} = jh_{y,\nu}, \ j = -n_{y,\nu}, ..., N_{y,\nu}, \quad h_{y,\nu} = L_\nu/N_{y,\nu}, \quad \nu = 1, 2, \end{aligned} \tag{3.1}$$

where integers $N_{x,\nu}$, $N_{y,\nu}$ set the number of grid points in domains D_ν, $\nu = 0, 1, 2$. Integer parameters $n_{y,\nu}$, $\nu = 1, 2$ determine the extent of overlapping between numerical grids in D_ν and D_0.

In order to obtain efficient stabilization to steady-state, we employed an implicit approximation of (2.2) in time and developed an approximate factorization method for decomposed computational domain. Different approximate factorization of finite-difference approximations to the system (2.2) were used in the central collecting pipe and in the inlet branch pipes. In D_0 the corresponding system of finite-difference equations is

$$\begin{aligned} &(A_t + \tau G_{x,0,i,j}^{(1,2,n)})(E + \tau A_t^{-1} G_{y,0,i,j}^{(1,2,n)}) \frac{U_{i,j}^{(n+1)} - U_{i,j}^{(n)}}{\tau} \\ &\quad + F_{x,0,i,j}^{(s,n)} + F_{y,0,i,j}^{(s,n)} = H_{xx,0,i,j}^{(q,n)} + H_{yy,0,i,j}^{(q,n)} \end{aligned} \tag{3.2}$$

while in D_ν, $\nu = 1, 2$, it is

$$\begin{aligned} &(A_t + \tau G_{y,\nu,i,j}^{(1,2,n)})(E + \tau A_t^{-1} G_{x,\nu,i,j}^{(1,2,n)}) \frac{U_{i,j}^{(n+1)} - U_{i,j}^{(n)}}{\tau} \\ &\quad + F_{x,\nu,i,j}^{(s,n)} + F_{y,\nu,i,j}^{(s,n)} = H_{xx,\nu,i,j}^{(q,n)} + H_{yy,\nu,i,j}^{(q,n)} + H_{xy,\nu,i,j}^{(q,n)}. \end{aligned} \tag{3.3}$$

Here $E = \text{diag}(1, 1, 1)$ is the identity matrix, $\tau = t^{(n+1)} - t^{(n)}$ is the time step, and $U_{i,j}^{(n)} = U(t^{(n)}, x_i, y_j)$ is a usual notation for grid functions. Approximation (3.2) is written for all interior grid points, i.e., for $(i,j) \in \{-N_{x,0} + 1, ..., N_{x,0} - 1\} \times \{-N_{y,0} + 1, ..., N_{y,0} - 1\}$ and (3.3) for $(i, j) \in \{-N_{x,\nu} + 1, ..., N_{x,\nu} - 1\} \times \{-n_{y,\nu} + 1, ..., N_{y,\nu} - 1\}$.

The finite-difference expressions $F_{\mu,\nu,i,j}^{(s,n)} = F_{\mu,\nu}^{(s)}(U_{i,j}^{(n)})$, $s = 1, 3, 5$, are the s-order upwind approximations to the derivatives $\partial W_{\nu,\mu}/\partial \mu_\nu$, $\mu \in \{x, y\}$, correspondingly. Terms $H_{\mu,\nu,i,j}^{(q,n)} = H_{\nu,\mu}^{(q)}(U_{i,j}^{(n)})$, $\mu \in \{xx, yy, xy\}$, designate the central difference approximation of the second $q = 2$ or fourth $q = 4$ order to the right-hand side of (2.2). The factorized finite-difference operators are defined by

$$G_{\mu,\nu,i,j}^{(s,q,n)} = \left.\frac{\partial F_{\mu,\nu}^{(s)} + H_{\mu\mu,\nu}^{(q)}}{\partial U}\right|_{U = U_{i,j}^{(n)}}, \quad \mu \in \{x, y\}, \ \nu = 0, 1, 2,$$

and were only used with $s = 1$ and $q = 2$, regardless of the values of these indexes in terms F and H in (3.2) and (3.3).

Our upwind approximations are exactly the same as proposed in [17]. For the lowest order of approximation to the term $\partial W_{x,\nu}/\partial x_\nu$ we have, for example,

$$F^{(1,n)}_{x,\nu,i,j} = (2h_{x,\nu})^{-1}\,[W^{(n)}_{x,\nu,i+1,j} - W^{(n)}_{x,\nu,i-1,j} - (A^{(+,n)}_{x,\nu,i+1/2,j} - A^{(-,n)}_{x,\nu,i+1/2,j})(U^{(n)}_{i+1,j} - U^{(n)}_{i,j}) + (A^{(+,n)}_{x,\nu,i-1/2,j} - A^{(-,n)}_{x,\nu,i-1/2,j})(U^{(n)}_{i,j} - U^{(n)}_{i-1,j})], \quad (3.4)$$

where $A^{\pm}_{x,\nu} = \frac{1}{2}S_{x,\nu}(\Lambda_{x,\nu} \pm |\Lambda_{x,\nu}|)S^{-1}_{x,\nu}$ and $S_{x,\nu}$ is the matrix of the similarity transform which diagonalizes $A_{x,\nu} = \partial W_{x,\nu}/\partial U = S_{x,\nu}\Lambda_{x,\nu}S^{-1}_{x,\nu}$. The half-integer value of an index, for example $i \pm \frac{1}{2}$, indicates that the corresponding matrix has to be computed with $U^{(n)}_{i\pm1/2,j} = \frac{1}{2}(U^{(n)}_{i+1/2\pm1/2,j} + U^{(n)}_{i-1/2\pm1/2,j})$. For the system (2.2)–(2.4),

$$S_{x,\nu} = \begin{pmatrix} 0 & \beta\xi_{x,\nu} & -\beta\xi_{x,\nu} \\ (-1)^\nu \cot\alpha_\nu & v_x(\eta_{x,\nu} + \xi_{x,\nu}) + \beta & v_x(\eta_{x,\nu} - \xi_{x,\nu}) + \beta \\ 1 & v_y(\eta_{x,\nu} + \xi_{x,\nu}) - (-1)^\nu\beta\cot\alpha_\nu & v_y(\eta_{x,\nu} - \xi_{x,\nu}) - (-1)^\nu\beta\cot\alpha_\nu \end{pmatrix},$$

$$S_{y,\nu} = \begin{pmatrix} 0 & \beta\xi_{y,\nu} & -\beta\xi_{y,\nu} \\ 1 & v_x(v_y + \xi_{y,\nu}) & v_x(v_y - \xi_{y,\nu}) \\ 0 & v_y(v_y + \xi_{y,\nu}) + \beta & v_y(v_y - \xi_{y,\nu}) + \beta \end{pmatrix},$$

and

$$\Lambda_{x,\nu} = \mathrm{diag}\,(\eta_{x,\nu}, \eta_{x,\nu} + \xi_{x,\nu}, \eta_{x,\nu} - \xi_{x,\nu})^{\mathrm{T}},$$
$$\Lambda_{y,\nu} = \mathrm{diag}\,(v_y, v_y + \xi_{y,\nu}, v_y - \xi_{y,\nu})^{\mathrm{T}},$$

where $\eta_{x,\nu} = v_x - (-1)^\nu v_y \cot\alpha_\nu$, $\xi_{x,\nu} = \sqrt{\eta^2_{x,\nu} + \beta(1 + \cot^2\alpha_\nu)}$, $\xi_{y,\nu} = \sqrt{v_y^2 + \beta}$.

Formulas for higher order approximations are available in [17] for a general curvilinear coordinate system in 3D. A simplified case is not repeated here. Approximations of properly decreased orders s and q were employed in the grid points which are close to the pipe walls as the high order formulas were used in the grid points which are at sufficient distance from the walls. However, the accuracy was kept at the level of the second-order approximation by waiving the upwind approximation at the grid points neighboring the boundaries. Namely, in accordance with [17], the formula

$$F^{(1,n)}_{x,\nu,i,j} = (2h_{x,\nu})^{-1}[W^{(n)}_{x,\nu,i+1,j} - W^{(n)}_{x,\nu,i-1,j} - \varepsilon(A^{(+,n)}_{x,\nu,i+1/2,j} - A^{(-,n)}_{x,\nu,i+1/2,j})(U^{(n)}_{i+1,j} - U^{(n)}_{i,j}) + \varepsilon(A^{(+,n)}_{x,\nu,i-1/2,j} - A^{(-,n)}_{x,\nu,i-1/2,j})(U^{(n)}_{i,j} - U^{(n)}_{i-1,j})],$$

with $\varepsilon = 0.01$, was employed there instead of (3.4).

At each time step the system (3.2), (3.3) is solved by the LU-decomposition of block-tridiagonal matrices $(A_t + \tau G^{(1,n)}_{x,0,i,j})$, $(E + \tau A_t^{-1} G^{(1,n)}_{y,0,i,j})$, $(A_t + \tau G^{(1,n)}_{x,\nu,i,j})$, and $(E + \tau A_t^{-1} G^{(1,n)}_{y,\nu,i,j})$ with the use of proper relationships at the boundaries of the computational subdomains. The sequence of computations involved in this procedure is illustrated in Fig. 3.1.

First, (3.2) is solved with respect to $w_{y,0} = (E + \tau A_t^{-1} G^{(1,n)}_{y,0,i,j})(U^{(n+1)}_{i,j} - U^{(n)}_{i,j})$ and (3.3) with respect to $w_{x,\nu} = (E + \tau A_t^{-1} G^{(1,n)}_{x,\nu,i,j})(U^{(n+1)}_{i,j} - U^{(n)}_{i,j})$. By doing so, we suppose that both $w_{y,0}$ and $w_{x,\nu}$ equal zero at the corresponding boundaries of the computational domains, i.e., at $i = \pm N_{x,0}$ and $j = -n_{y,\nu}, N_{y,\nu}$, $\nu = 1, 2$. This assumption, restricting the approximation order by $O(\tau)$, is crude for nonstationary solutions certainly, but it is exact for the steady-state versions and was used in stabilization successfully.

Second, equations $(E + \tau A_t^{-1} G^{(1,n)}_{y,\nu,i,j})(U^{(n+1)}_{i,j} - U^{(n)}_{i,j}) = w_{x,\nu}$, $\nu = 1, 2$, are solved with respect to $U^{(n+1)}_{i,j} - U^{(n)}_{i,j}$ in D_1 and D_2 for $j = 0, \ldots, N_{y,\nu} - 1$. Here zero flow velocity at the pipe walls is specified as a boundary condition and one further approximate relation is added in order to close up the system of grid equations. The need for this additional relationship emanates from the use of noncompact finite-difference approximations to the system (2.2)–(2.4). This closing relationship has been formed from the equation of conservation of the x_ν-component of momentum. At the pipe walls it appears as

$$\frac{\partial p}{\partial x_\nu} = \frac{1}{\mathrm{Re}}\left\{(1 + \cot^2\alpha_\nu)\frac{\partial^2 v_x}{\partial x_\nu^2} - 2(-1)^\nu \cot\alpha_\nu \frac{\partial^2 v_x}{\partial x_\nu \partial y_\nu}\right\} \quad (3.5)$$

and was approximated by the second-order formula

$$\pm(p^{(n+1)}_{\pm N_{x,\nu},j} - p^{(n+1)}_{\pm N_{x,\nu}\mp1,j}) = \mp\frac{1}{2}(p^{(n)}_{\pm N_{x,\nu},j} - 2p^{(n)}_{\pm N_{x,\nu}\mp1,j} + p^{(n)}_{\pm N_{x,\nu}\mp2,j}) - \frac{1 + \cot^2\alpha_\nu}{h_{x,\nu}\mathrm{Re}}$$
$$(5v^{(n)}_{x,\pm N_{x,\nu}\mp1,j} - 4v^{(n)}_{x,\pm N_{x,\nu}\mp2,j} + v^{(n)}_{x,\pm N_{x,\nu}\mp3,j}) \pm \frac{(-1)^\nu\cot\alpha_\nu}{2h_{y,\nu}\mathrm{Re}}$$
$$(4v^{(n)}_{x,\pm N_{x,\nu}\mp1,j+1} - v^{(n)}_{x,\pm N_{x,\nu}\mp2,j+1} - 4v^{(n)}_{x,\pm N_{x,\nu}\mp1,j-1} + v^{(n)}_{x,\pm N_{x,\nu}\mp2,j+1}). \quad (3.6)$$

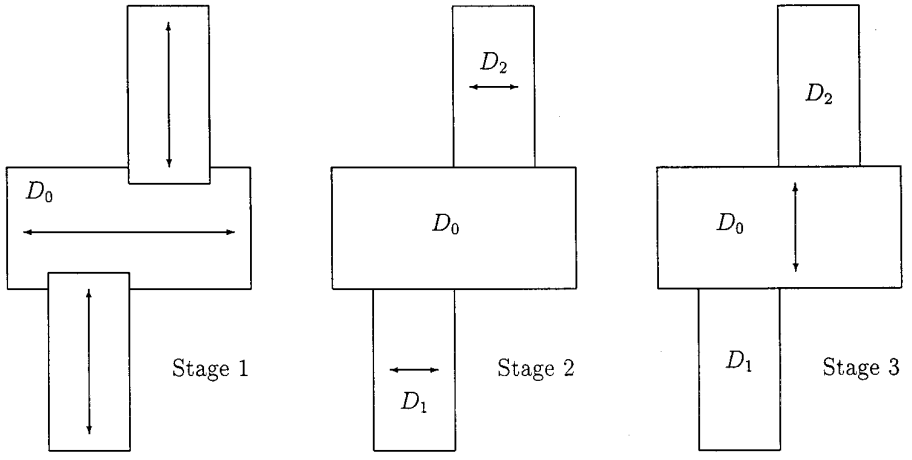

FIG. 3.1. Sequence of sweeps during each time step.

In corner points almost the same formulas, but explicit and averaged for D_ν and D_0 (see (3.10)), were used.

Computation of $U^{(n+1)}_{i,N_{y,\nu}} - U^{(n)}_{i,N_{y,\nu}}$ is carried out by a special procedure. Here, two boundary conditions (2.11) have been approximated and one further equation obtained by discretization of the characteristic relationship corresponding to the characteristic of (2.2)-(2.4) coming from the interior of D_ν along the lines $x_\nu = \text{const}$ has been added. This additional equation was written in the form

$$\frac{1}{2}(E + |\Lambda_{y,\nu}|\Lambda^{-1}_{y,\nu})S^{-1}_{y,\nu}\left\{A_t\frac{\partial U}{\partial t} + \frac{\partial W_{x,\nu}}{\partial x_\nu} + \frac{\partial W_{y,\nu}}{\partial y_\nu}\right.$$
$$\left. - \mathrm{Re}^{-1}B\left[(1+\cot^2\alpha_\nu)\frac{\partial^2 U}{\partial x_\nu^2} - 2\cot\alpha_\nu\frac{\partial^2 U}{\partial x_\nu \partial y_\nu} + \frac{\partial^2 U}{\partial y_\nu^2}\right]\right\} = 0,$$
$$(x_\nu, y_\nu) \in D_\nu, t > 0, \nu = 1, 2, \quad (3.7)$$

and was approximated by the same scheme as the system (2.2). All required formulas have been given earlier in this section. Values of functions in the grid points exterior to D_ν were refilled by the Lagrange interpolation formula. The integrals in (2.11) were approximated by Simpson's rule.

Approximation of (3.7) with both (2.11) and (2.13), (2.14) may be reduced to the system of linear equations

$$\begin{bmatrix}
\Omega_{0,0} & \Omega_{0,1} & 0 & 0 & \cdots & 0 & \varphi_0 \\
\Omega_{1,-1} & \Omega_{1,0} & \Omega_{1,1} & 0 & \cdots & 0 & \varphi_1 \\
0 & \Omega_{2,-1} & \Omega_{2,0} & \Omega_{2,1} & \cdots & 0 & \varphi_2 \\
\cdots & \cdots & \cdots & \cdots & \cdots & \cdots & \cdots \\
0 & \cdots & 0 & \Omega_{m-1,-1} & \Omega_{m-1,0} & \Omega_{m-1,1} & \varphi_{m-1} \\
0 & \cdots & 0 & 0 & \Omega_{m,-1} & \Omega_{m,0} & \varphi_m \\
\psi_0 & \cdots & \psi_{m-3} & \psi_{m-2} & \psi_{m-1} & \psi_m & \Omega
\end{bmatrix}
\begin{bmatrix} \zeta_0 \\ \cdot \\ \cdot \\ \cdot \\ \zeta_m \\ z \end{bmatrix} =
\begin{bmatrix} g_0 \\ \cdot \\ \cdot \\ \cdot \\ g_m \\ \gamma \end{bmatrix}, \quad (3.8)$$

where all entries are scalars. Corresponding formulas are rather cumbersome and are not cited here for the sake of brevity.

The matrix of the system (3.8) is different of usual band matrixes, but it can be still efficiently solved demanding $O(N_{x,\nu})$ arithmetic operations. A suitable algorithm is given below:

$$\omega_0 = -\Omega^{-1}_{0,0}\Omega_{0,1}, \quad \kappa = -\Omega^{-1}_{0,0}\varphi_0, \quad \chi = \Omega^{-1}_{0,0}g_0,$$
$$\omega_i = -(\Omega_{i,-1}\omega_{i-1} + \Omega_{i,0})^{-1}\Omega_{i,1},$$
$$\kappa_i = -(\Omega_{i,-1}\omega_{i-1} + \Omega_{i,0})^{-1}(\Omega_{i,-1}\kappa_{i-1} + \varphi_i),$$
$$\chi_i = -(\Omega_{i,-1}\omega_{i-1} + \Omega_{i,0})^{-1}(\Omega_{i,-1}\chi_{i-1} - g_i), \quad i = 1, ..., m,$$
$$\vartheta_m = \kappa_m, \quad \eta_m = \chi_m,$$
$$\vartheta_i = \kappa_i + \omega_i\vartheta_{i+1}, \quad \eta_i = \chi_i + \omega_i\eta_{i+1}, \quad i = m-1, ..., 0,$$
$$z = \left(\Omega + \sum_{i=0}^{m}\psi_i\vartheta_i\right)^{-1}\left(\gamma - \sum_{i=0}^{m}\psi_i\eta_i\right),$$
$$\zeta_i = \vartheta_i z + \eta_i, \quad i = 0, ..., m. \quad (3.9)$$

During the third stage the system of equations $(E + \tau A_t^{-1}G^{(1,n)}_{y,0,i,j})(U^{(n+1)}_{i,j} - U^{(n)}_{i,j}) = w_{y,0}$ is solved with respect to $U^{(n+1)}_{i,j} - U^{(n)}_{i,j}$. Zero velocity and a closing relationship

formed from the equation of conservation of the y_0-component of momentum have been specified at the pipe walls again. The corresponding formula is an obvious simplification of (3.5):

$$\frac{\partial p}{\partial y_0} = \frac{1}{\mathrm{Re}} \frac{\partial^2 v_y}{\partial y_0^2}.$$

Its finite-difference approximation comes easily by analogy with (3.6):

$$\begin{aligned} &\pm(p^{(n+1)}_{i,\pm N_{y,0}} - p^{(n+1)}_{i,\pm N_{y,0}\mp 1}) \\ &= \mp\frac{1}{2}(p^{(n)}_{i,\pm N_{y,0}} - 2p^{(n)}_{i,\pm N_{y,0}\mp 1} + p^{(n+1)}_{i,\pm N_{y,0}\mp 2} \\ &\quad - \frac{1}{h_{y,0}\,\mathrm{Re}}(5v^{(n)}_{y,i,\pm N_{y,0}\mp 1} - 4v^{(n)}_{y,i,\pm N_{y,0}\mp 2} + v^{(n)}_{y,i,\pm N_{y,0}\mp 3}). \end{aligned} \tag{3.10}$$

Here, special attention was paid not only to the computation of $U^{(n+1)}_{\pm N_{x,0},j} - U^{(n+1)}_{\pm N_{x,0},j}$, but also to the treatment of equations $(E + \tau A_t^{-1} G^{(1,n)}_{y,0,i,j})(U^{(n+1)}_{i,j} - U^{(n)}_{i,j}) = w_{y,0}$ along the grid lines, $x_{0,i} = \mathrm{const}$, which have common points with the boundaries of D_1 and D_2. In order to solve grid equations along these lines, values of $U^{(n+1)}_{i,0}$, computed at the second stage, have been used as the boundary conditions on the common boundaries of D_0 and D_ν, $\nu = 1, 2$. The reciprocal influence of the flow in D_0 on that ones in the inlet branches was taken into account on completion of the third stage by redefinition of $U^{(n+1)}_{i,j}$ for $-n_{y,\nu} \le j < 0$ in the extension of D_ν, $\nu = 1,2$, to D_0. New values of flow parameters in grid points exterior to D_ν were obtained by using high order interpolation splines and values of the flow parameters $U^{(n+1)}_{i,j}$ in nodes of the numerical grid in D_0. These interpolated flow parameters are used in computations in D_ν, $\nu = 1, 2$, during the first stage of the next time step. Specifying the chosen coordinate system reduces the interpolation to essentially one dimension. Moreover, for certain values of the parameters, grid nodes of overlapping subdomains are the same and interpolation is not required at all.

Computation of $U^{(n+1)}_{\pm N_{x,0},j} - U^{(n)}_{\pm N_{x,0},j}$ at the outlets was carried out in the same manner as the computation of $U^{(n+1)}_{i,N_{y,\nu}} - U^{(n)}_{i,N_{y,\nu}}$ at the inlets. The boundary condition (2.12) or (2.15) has been approximated and a system of two finite-difference equations obtained by discretization of the characteristic relationships corresponding to the characteristics of (2.2)–(2.4) coming from the interior of D_0 along the lines $y_0 = \mathrm{const}$ has been added. Similarly to the inlet flow, the resulting system of finite-difference equations may be reduced to the system (3.8) with properly defined entries. In this case the finite-difference systems for both outlets are coupled and all the entries of the matrix of the system (3.8) will be 2×2 matrixes, if $R_p \neq 0$. However, the solution algorithm (3.9) is still suitable and efficient in this case too.

The march along the artificial time t (or iterations with respect to index n) proceeds until the stabilization parameter

$$\varepsilon^{(n+1)} = \tau^{-1} \max_{i,j} \left\{ \frac{|p^{(n+1)}_{i,j} - p^{(n)}_{i,j}|}{|p^{(n)}_{i,j}| + \delta_0}, \frac{\|\mathbf{v}^{(n+1)}_{i,j} - \mathbf{v}^{(n)}_{i,j}\|}{\|\mathbf{v}^{(n)}_{i,j}\| + \delta_0} \right\} \tag{3.11}$$

becomes less than some given value ε_0. Parameter $\delta_0 > 0$ prevents division by zero occurring and $\mathbf{v}$ denotes the velocity vector (v_x, v_y).

4. COMPUTATIONAL RESULTS

A set of computations of fluid flows in T- and X-geometries was carried out. Values of $\Delta l \in [0,2d_0]$, $\alpha_1 = 90°$, and $\alpha_2 \in [50°, 130°]$, where d_0 is the diameter of the inlet and outlet branch pipes considered. The Reynolds number was in the range [100, 1000]. The length of the central pipe was $10d_0$. The inlet branch pipes were located symmetrically around the center of the outlet pipe having $5d_0$ length. Most of the computations were carried out using numerical grids consisting of 11×101 (in D_0) and of 11×51 (in $D_{1,2}$) nodes for $h_1 = h_{x,\nu} = h_{y,\nu} = 0.1$. Finer numerical grids with $h_2 = h_{x,\nu} = h_{y,\nu} = 0.05$ and $h_3 = h_{x,\nu} = h_{y,\nu} = 0.025$ were used in order to check accuracy of the algorithm in practice.

For $\mathrm{Re} \le 700$ the value of $\varepsilon_0 = 10^{-3}$ in (3.11) gives satisfactory results. The number of time steps required to obtain steady-state solutions was in the range 100 to 5000, depending on the approximation order of the numerical algorithm, the geometry of the junction, and on the Reynolds number. Stabilization speed is crucially decreased if Re exceeds some critical value, which depends on the geometry of the flow. Usually, this value is greater than 1000, but for some configurations it may be as small as about 800. In general, it is possible to say that the critical Reynolds number is greater than 700 for flows considered in this work. Such deterioration of convergence to steady state is not surprising for Reynolds numbers approaching a threshold of stability of steady-state regime. It may have a very complex nature and deserves, probably, a separate consideration.

In computational experiments values of the time step were chosen as $\tau = ch$. It was possible to conduct most of the computations with the first-order scheme for $c = 50$. The third- and fifth-order schemes have required values of c not greater than 40 and 10, respectively, in the best cases. It was found that the minimal extent of grid overlapping, corresponding to $n_{y,\nu} = -1$, is near the optimum. The computational program was written in Fortran-77 and the available computer code elapses every time step approxi-

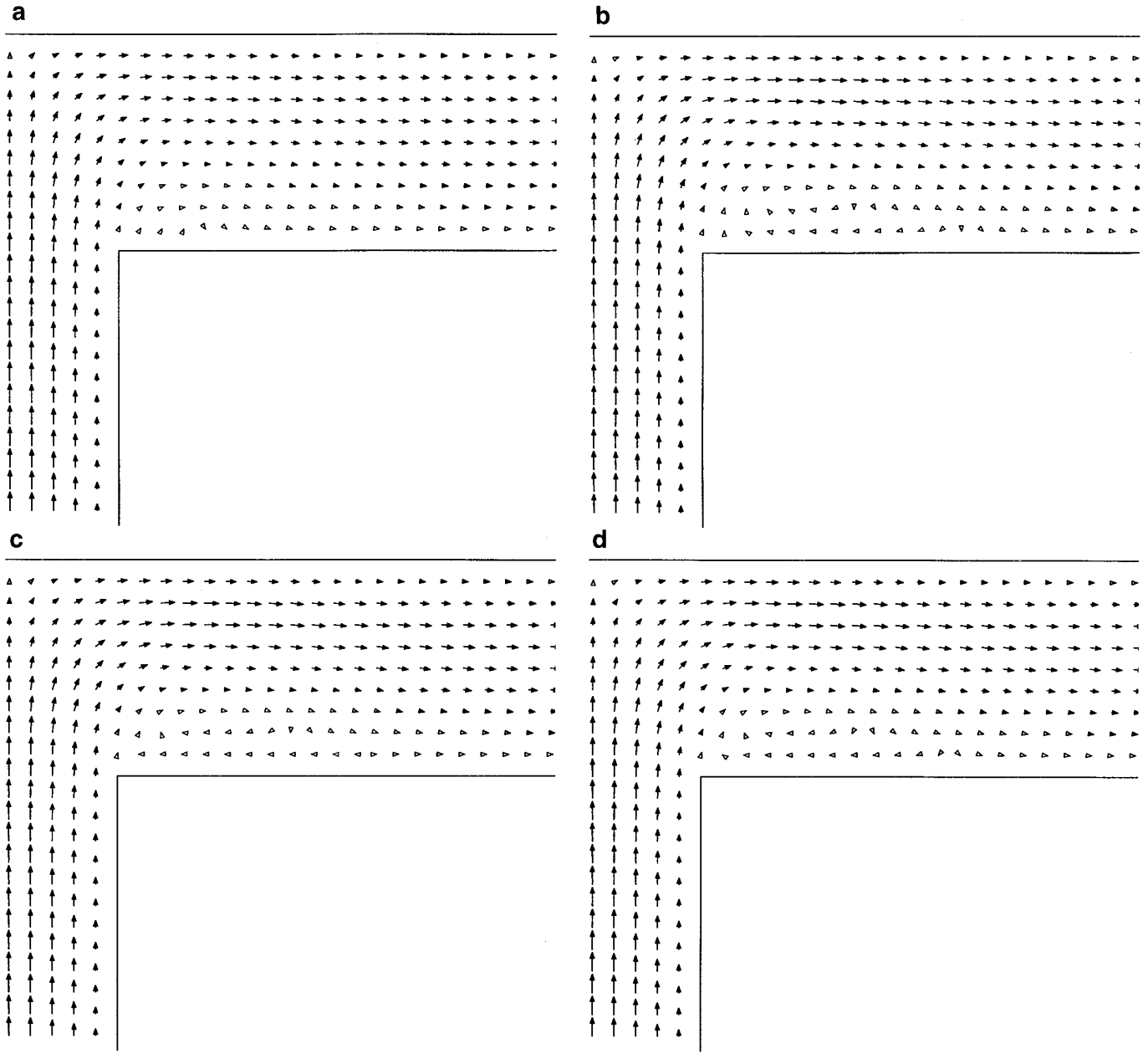

FIG. 4.1. Influence of the order of approximation and the grid step size on calculated velocity vector field: (a) First order, $h = 0.1$; (b) third order, $h = 0.1$; (c) fifth order, $h = 0.1$; (d) fifth order, $h = 0.025$; (e) third order, $h = 0.05$; (f) fifth order, $h = 0.05$.

mately 6×10^{-4} s of "wall clock" time per grid node on Sun SPARC-10/51 with one processor.

In order to explore the efficient accuracy of the proposed algorithms, values of the parameter

$$\sigma_{i,j} = \log_2 \left\{ \max \left[\frac{|p_{h_1}(ih_1, jh_1) - p_{h_2}(ih_1, jh_1)|}{|p_{h_2}(ih_1, jh_1) - p_{h_3}(ih_1, jh_1)| + \delta_0}, \frac{\|\mathbf{v}_{h_1}(ih_1, jh_1) - \mathbf{v}_{h_2}(ih_1, jh_1)\|}{\|\mathbf{v}_{h_2}(ih_1, jh_1) - \mathbf{v}_{h_3}(ih_1, jh_1)\| + \delta_0} \right] \right\} \tag{4.1}$$

were analyzed for some steady-state flow cases. Theoretically, $\sigma_{i,j}$ should equal 1, 3, and 5 for the first-, third-, and fifth-order schemes, respectively. In practice, its values were slightly different than 1 for the first-order scheme and reasonably close to 3 in almost all grid points except for small regions around the corner points in the third-order algorithm. For the fifth-order scheme the value of $\sigma_{i,j}$ was not less than 4.3 in the grid points distant from the pipe walls. However, the value of the effective approximation order was considerably less (below 3) at the pipe walls

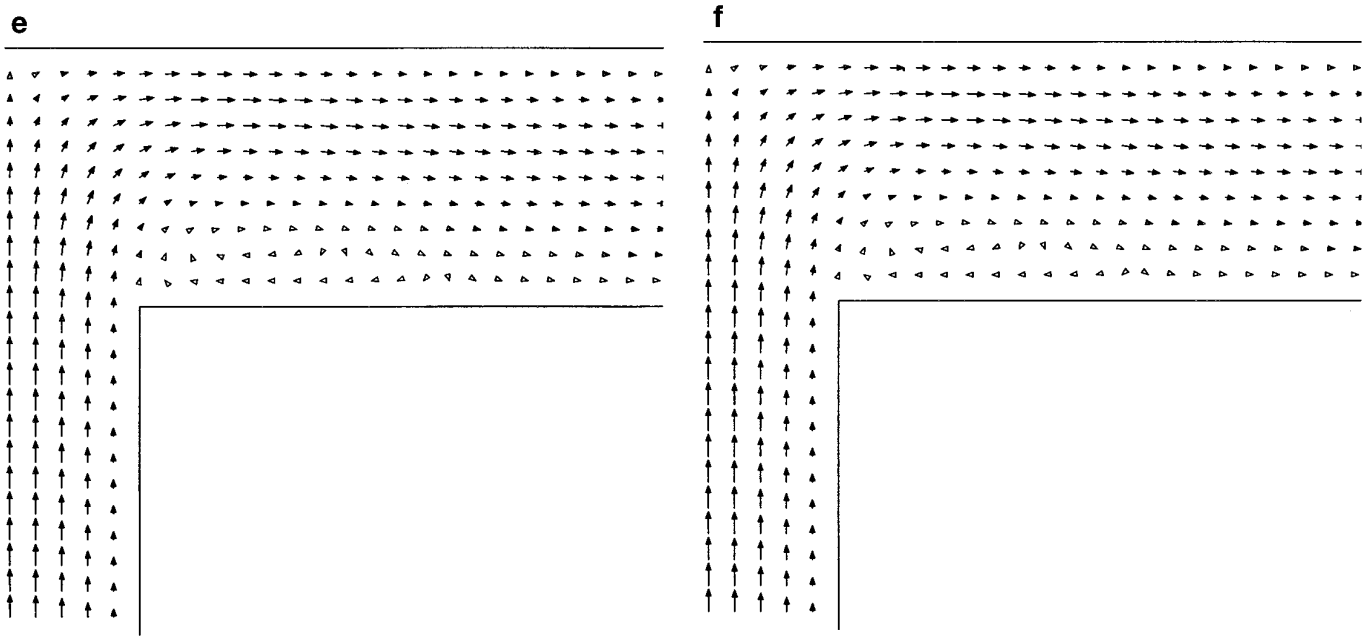

FIG. 4.1. (*continued*)

and even less than 2 in the corner points. An important observation ascertained in this analysis is that approximation errors remain local, in practice.

Figures 4.1a–4.1c illustrate the influence of the order of approximation of the scheme on the velocity vector field in a T-junction for the numerical grid with $h_{x,\nu} = h_{y,\nu} = 0.1$. A set of Figs. 4.1c, f, d shows the dependence of the numerical solution on the grid step size for the fifth-order scheme. Figure 4.1e completes the picture, providing the velocity field obtained with the third-order scheme for $h_{x,\nu} = h_{y,\nu} = 0.05$. These figures visually demonstrate that the third-order scheme is quite accurate and the fifth-order one does not provide improvement of accuracy on the crude grid $h_{x,\nu} = h_{y,\nu} = 0.1$. However, the advantage becomes apparent on finer grids with steps $h_{x,\nu}$, $h_{y,\nu} \le 0.05$, while it is difficult to observe visually. It should be taken into account that the fifth-order algorithm involves many more computations per time step and imposes considerably more severe restrictions on the value of τ, resulting in slower stabilization to the steady state. Probably, the third-order algorithm is a more robust one, at least on crude grids.

In the original work [4], the parameter of artificial compressibility β was introduced as a coefficient at the divergence of the velocity vector. This parameter influences the relaxation speed crucially but its involvement in the flux-difference splitting may result in severe numerical dissipation and dispersion. In particular, for the first-order scheme the residual of the finite-difference approximation includes a numerical dissipation term $2^{-1}hA_{xx}^{(h)}\partial^2 U/\partial x^2$, where

$$A_{xx}^{(h)} = \begin{pmatrix} \dfrac{\beta}{\sqrt{\beta+v_x^2}} & \dfrac{\beta v_x}{\sqrt{\beta+v_x^2}} & 0 \\ \dfrac{v_x}{\sqrt{\beta+v_x^2}} & \dfrac{\beta+2v_x^2}{\sqrt{\beta+v_x^2}} & 0 \\ \dfrac{v_y(\sqrt{\beta+v_x^2}-|v_x|)}{\sqrt{\beta+v_x^2}} & \dfrac{v_x v_y(2\sqrt{\beta+v_x^2}-|v_x|)}{\sqrt{\beta+v_x^2}} & -|v_x| \end{pmatrix}.$$

In stagnation points this term has an asymptotics as $2^{-1}h\sqrt{\beta}\ \mathrm{diag}(1, 1, 0)\partial^2 U/\partial x^2$ which is quite competitive with natural dissipation $\mathrm{Re}^{-1}\ \mathrm{diag}(0, 1, 1)\partial^2 U/\partial x^2$ for large values of β, h, and Re.

Figure 4.2a shows the effect of $\beta = 10$ in the same situation as depicted in Fig. 4.1a, where $\beta = 1$. The influence of β is much less for high order schemes using flux-difference splitting, but it is still trackable in near to stagnation regions as can be seen in Fig. 4.2b, where the flow was calculated with $\beta = 10$ and the same other conditions as those plotted in Fig. 4.1c.

Algorithms presented in this paper use parameters of artificial compressibility β_p, β_x, β_y as coefficients at the time derivatives (2.2)–(2.4) without involving them in the flux-difference splitting. This approach corresponds to the general idea of preconditioning by scaling variables [6]. In the case of a system of linear algebraic equations $\mathscr{A}u = f$ it consists in transformation of the system $\mathscr{A}u = f$ into an equivalent system $\mathscr{D}_1\mathscr{A}\mathscr{D}_2^{-1}v = \mathscr{D}_1 f$, where $\mathscr{D}_1$ and $\mathscr{D}_2$ are

diagonal matrices and $v = \mathscr{D}_2 u$. The stabilization method applied to the transformed system may be written as

$$\mathscr{D}_1^{-1}\frac{dV}{dt} + \mathscr{A}\mathscr{D}_2^{-1}V = f,$$

which takes the form, after proper discretization,

$$\frac{V^{(n+1)} - V^{(n)}}{\tau} + \mathscr{T}V^{(n)} = f.$$

Matrix $\mathscr{T}$ depends on the chosen time-discretization. It may be, for example, $\mathscr{T} = \mathscr{D}_1\mathscr{A}\mathscr{D}_2^{-1}$ or $\mathscr{T} = (\mathscr{E} + \tau\mathscr{D}_1\mathscr{A}\mathscr{D}_2^{-1})^{-1}\mathscr{D}_1\mathscr{A}\mathscr{D}_2^{-1}$ for the explicit or implicit Euler finite-difference schemes, correspondingly. Choice of the matrices $\mathscr{D}_1$ and $\mathscr{D}_2$ should provide the fastest convergence of $V^{(n)}$ to $\mathscr{A}^{-1}f$ as $n \to \infty$. In our specific case $\mathscr{D}_1^{-1} = \mathrm{diag}(\mathrm{diag}(\beta_p, \beta_x, \beta_y), ..., \mathrm{diag}(\beta_p, \beta_x, \beta_y), ..., \mathrm{diag}(\beta_p, \beta_x, \beta_y))$ and $\mathscr{D}_2$ is the identity matrix. Operator $\mathscr{T}$ is rather complex because of factorization and decomposition.

We have carried out a set of test runs with different values of parameters β_p, β_x, and β_y. Typical results of the variation of β_p are shown in Table I as number of time steps required to reach certain stabilization level (3.11). Parameters β_x and β_y affect stabilization rate too, but a few test computations undertaken here could not reveal any more or less easily interpreted regularity. Alternatively, optimal values of all three parameters may be estimated numerically by direct minimization of cond($\mathscr{T}$) for a linearized problem in a simplified geometry, as β_p, β_x and β_y do not vary from node to node of the grid.

TABLE I

Influence of Parameter β_p on Convergence Rate ($\beta_x = \beta_y = 1$)

$\varepsilon^{(n)}/\beta_p$	0.05	0.1	0.2	1	2
10^{-3}	200	140	140	180	220
10^{-6}	460	360	380	420	500
10^{-9}	1260	740	820	1080	1540

Another approach to introduction of scaling parameters, together with theoretical analysis of their optimal values was considered in [20]. In [12] these theoretically optimal values were carefully checked by intensive Navier–Stokes computations. Our observations are in a qualitative agreement with results in [20, 12]. Some quantitative discrepancy may be explained by large Courant numbers used in this work, while the analysis in [20] holds for Courant numbers not exceeding 1 by very much. Moreover, computations in [12] confirmed the dependence of optimal β (which plays the same role as β_p^{-1}) on the computational algorithm.

The *T*-configuration was used as a debugging tool and test case in this work. Figure 4.3 illustrates a fluid flow in a symmetrical *T*-junction. Here and in the following figures we reproduce central parts of the computational domains only, because flow in the inlet and outlet regions was always

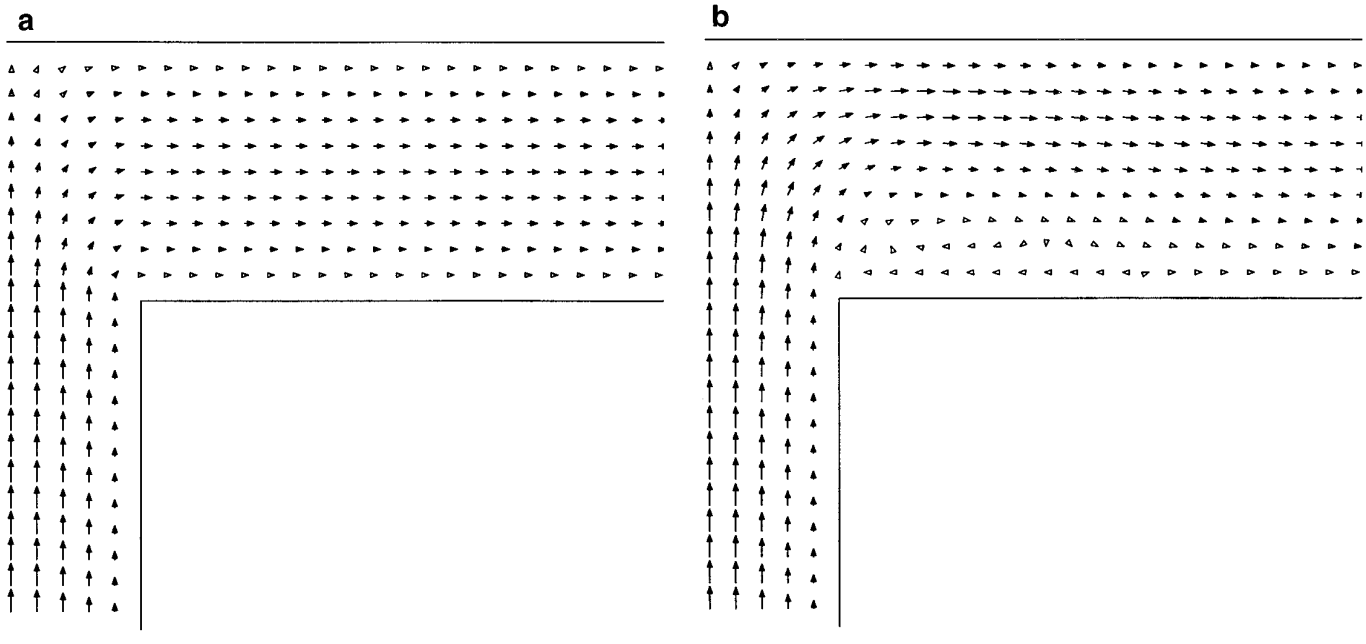

FIG. 4.2. Velocity vector fields calculated for $\beta = 10$: (a) First order, $h = 0.1$; (b) fifth order, $h = 0.1$.

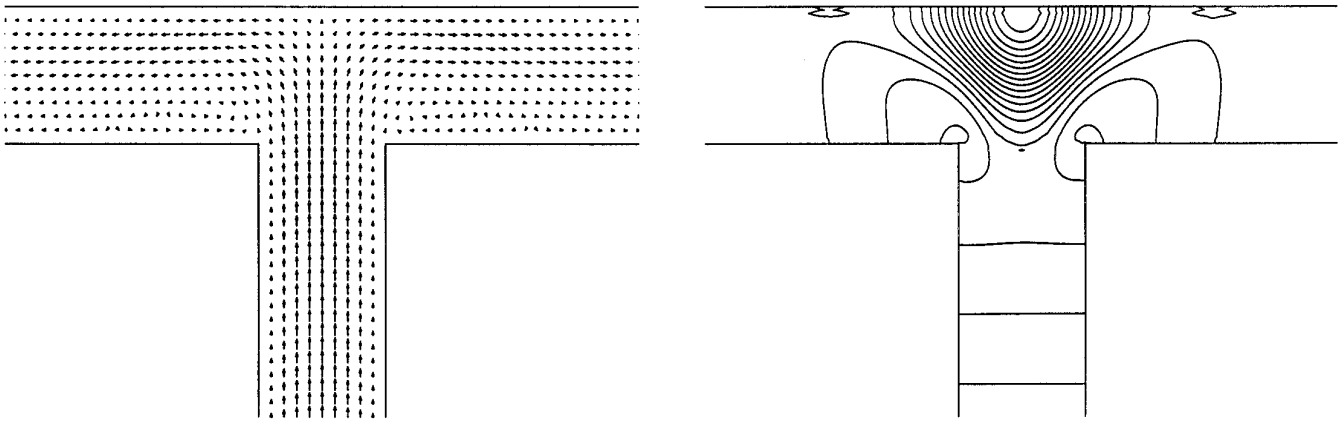

FIG. 4.3. Velocity vector field and pressure level lines in a T-junction, Re = 100.

uniform. Figure 4.3 may be compared to Fig. 3.2 from [1], where a similar flow was calculated for fixed values of pressure at the inlet and outlets.

An example of fluid flow in the symmetrical X-junction is shown in Fig. 4.4. The pressure in the center of the X-junction is essentially higher than in the T-junction. Probably, this is the main reason which prevents flow separation at the central pipe wall near the junction.

Proposed computational algorithms were used in numerical study of fluid flows in X-junctions related to the total cavopulmonary anastomosis in surgery of congenital heart anomalies [5]. This operation is efficient in some cases of severe disability of the right side of the heart. In particular, if its pumping function is degenerated and the right side of the heart creates an additional hydraulic resistance only, then it is expedient to bypass it. Two main techniques were proposed by the time being: the Fontan atriopulmonary connection and the total cavopulmonary anastomosis [5, 15]. The essence of the total cavopulmonary connection is illustrated in Fig. 1.3.

The energy resource of the human heart is strictly limited and only about 10% of the power of the left side of the heart is spent to move the blood in the pulmonary circulation if the right side of the heart is disabled. Therefore, even a

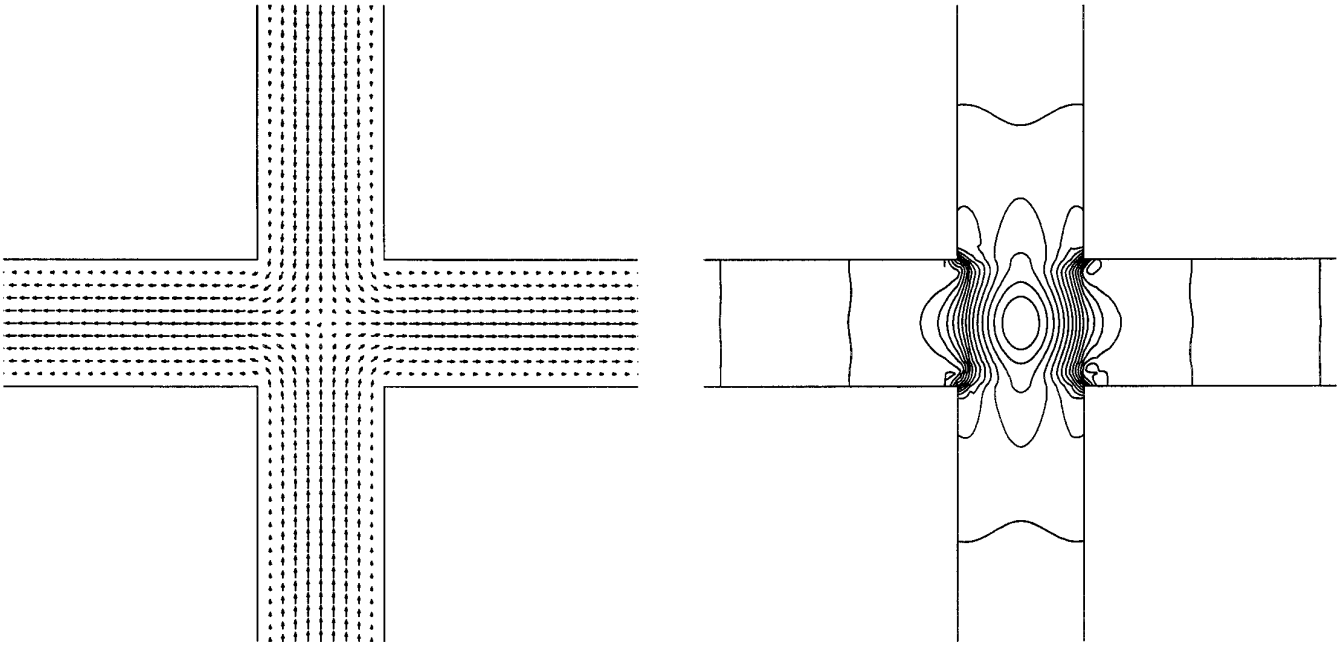

FIG. 4.4. Velocity vector field and pressure level lines in an X-junction, Re = 100.

small increase of the mass flow rate may be of vital importance in some cases and the cavopulmonary junction should be carefully optimized. On the other hand, the artificial junction should not lead to extra mechanical hemolysis. In this work the circulation system depicted in Fig. 1.2 was considered as a hydrodynamical model of the total cavopulmonary connection. There are three parameters to optimize, i.e., the inclination angles α_ν, $\nu = 1, 2$, and displacement Δl between the inlet branch pipes. The human anatomy imposes certain constraints on the admissible values of these parameters both in general and in particular.

In accordance with [2], the Reynolds number in the vena cava of a normal human is about 700 and the blood flow may be considered as that of a laminar flow of Newtonian liquid. Its dynamics is governed by the Navier–Stokes equations therefore. In children with an impaired right side of the heart, pulsations in the venous systemic circulation are not as important as in a normal human and the steady-state solutions of the Navier–Stokes system are reasonable approximations for flows in the cavopulmonary junction. Distensibility of the pipe walls has not been taken into account, because it is not essential in the absence of pulsations. Similar assumptions were admitted in the comparative experimental study of the Fontan atriopulmonary connection and the total cavopulmonary anastomosis reported in [11].

Thus, the only crucial assumption we admitted in this model is a 2D consideration of an essentially 3D flow case. This simplification is natural and expedient on certain stages of investigation of complicated problems. It provides valuable information on possible computational peculiarities and gives useful ideas on further refinements of the model. See, for example, [18], where the numerical investigation of pulsating flows in T-configurations was also undertaken in 2D geometry.

Values of hydraulic resistances were estimated using the data for pressure and blood mass flow rate in a normal human body [2]. In particular, the total resistance of the systemic circle was assumed to be 2.6×10^5 m$^{-1} \cdot$ s^{-1} and for the pulmonary circle, 3×10^4 m$^{-1} \cdot$ s^{-1}. The diameter of the right pulmonary artery $d_0 = 0.015$ m, the blood density $\varrho = 1$ kg $\cdot$ m^{-3} and an average flow velocity in the vena cava $V = 0.2$ m $\cdot$ s^{-1} were taken as basic units. Thus, assuming a symmetry of the circulation network, required resistances were estimated as $R_1 = R_2 = 585$ and $R_{01} = R_{02} = 67.5$. A zero value of R_p has also been assumed, resulting in $\mathscr{P} = 319$. There is no requirement to know absolute values of pressure in this problem and the value of $p_{in} = 0$ has been fixed. Typical computational results are presented in Figs. 4.5 and 4.6 for Re = 500.

The following general observations were obtained through a set of computations. The optimal value of the inclination angle α_2 is usually less than 90° and the optimal value of the displacement Δl is usually greater than 0 as well. However, at large values of the displacement, greater than approximately $0.9d_0$, a system of blocked vortices is likely to appear with increasing mechanical hemolysis and the probability of clot formation (see Figs. 4.5 and 4.6).

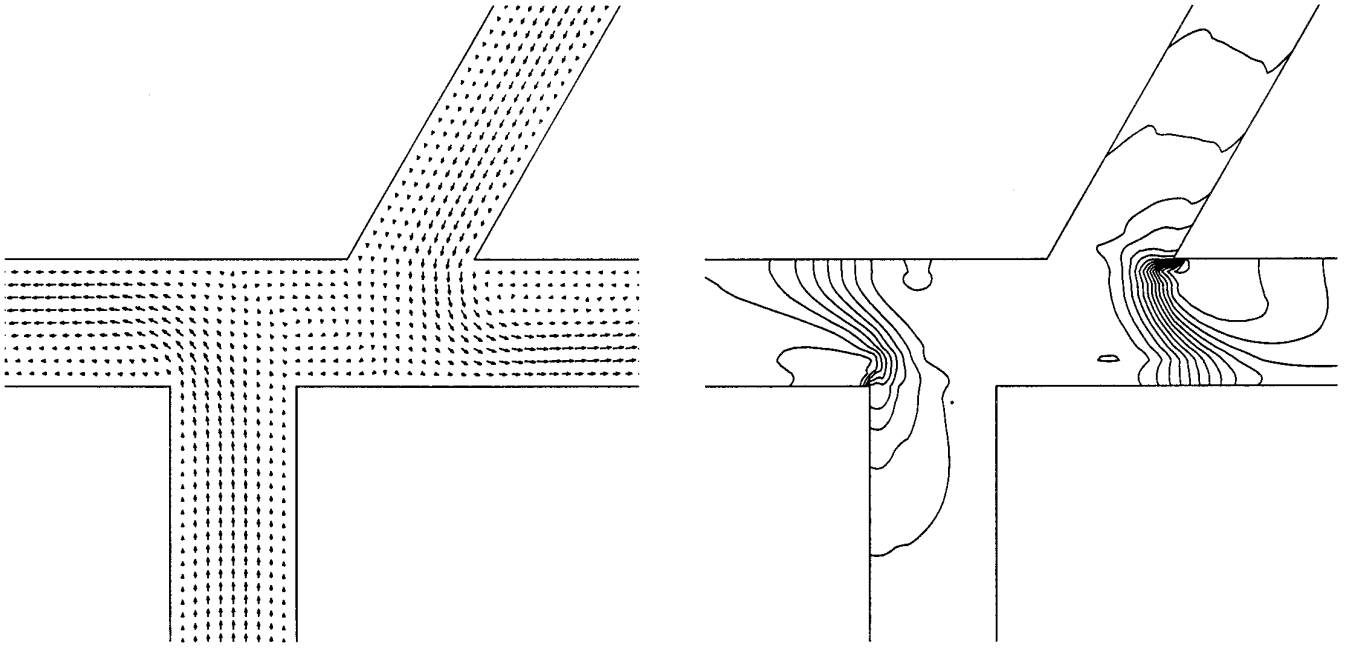

FIG. 4.5. Velocity vector field and pressure level lines in an X-junction, $\alpha_2 = 60°$.

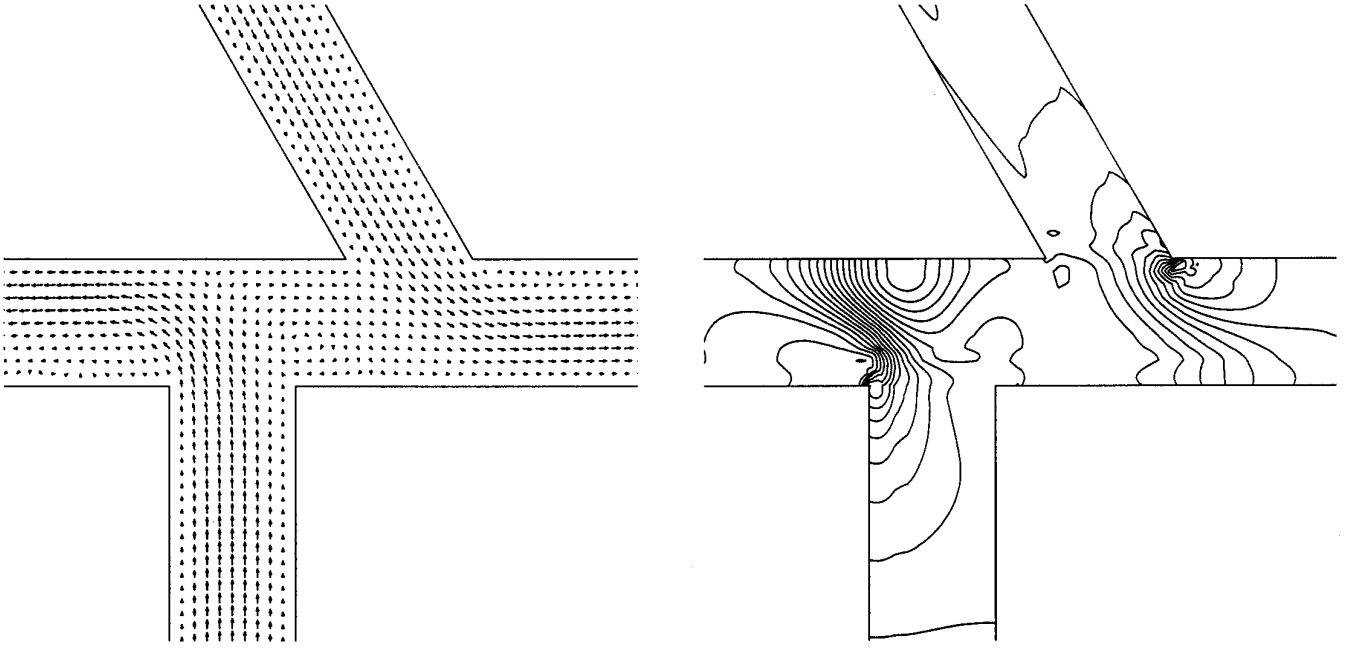

FIG. 4.6. Velocity vector field and pressure level lines in an X-junction, $\alpha_2 = 120°$.

Variations of the inclination angle α_1 are difficult in the practice of surgery and have not been considered in this investigation.

Beside free parameters $\alpha_{1,2}$ and Δl subjected to optimization, the proposed circulation model includes a set of given parameters $R_{1,2}$, $R_{01,02}$, R_p, $\mathscr{P}$, $d_{0,1,2}$, and Re. The values of these parameters, in particular, asymmetry in R_{01} and R_{02}, vary from case to case and may affect the results of optimization rather strongly. Additionally, variations in the location of veins and arteries make it impossible to give detailed universal recommendations. However, the efficiency of the model gives an opportunity to analyze every particular case promptly, on request.

As it was mentioned in Section 1, the main aim of this work is to combine two types of mathematical models of flows in pipe networks. In order to achieve this specific aim effectively, some components of numerical algorithms were intentionally simplified, resulting in the narrowing of their area of applicability. In particular, the simplicity of the employed numerical grids causes degradation of accuracy as $\alpha_{1,2}$ tends to 0° or 180°. However, more sophisticated numerical grids can be easily adapted in this method by using general space-discretization formulas from [17] and interpolation procedures from [3], if required.

Implementation of ADI algorithms in the case of decomposed geometries have required certain efforts in order to find a suitable sequence of sweeps in subdomains, ensuring fast convergence to the steady state. These efforts will be multiplied in three dimensions, indeed. However, recent work [16] shows that high efficiency of stabilization can be achieved by using algorithms based on very universal preconditioned GMRES solvers.

Besides refinement of computational algorithms, some developments of the physical flow model may be of interest for prospective research too. One of them is the employment of a detailed ''integral'' model of circulation network, like [19], instead of the simplest one proposed in this work. Also, it is important to advance the flow model towards time-dependent multiphase flow in order to get a chance to treat hemolysis and thrombosis quantitatively.

5. CONCLUSIONS

Robust high-order approximation methods intended to treat steady-state flows of viscous fluid in junctions of pipes of multicomponent circulation systems were developed.

Proposed methods were verified by solving a problem related to a surgical treatment of the cardiovascular system which is known as the total cavopulmonary anastomosis. Some useful observations in regard to optimization of the cavopulmonary connection were obtained. Unlike 2D consideration is obviously not enough for comprehensive solution of this problem, it proofs plausibility of the model of node–network interaction and efficiency of chosen computational approach.

Further directions of research in both refinement of the computational algorithms and physical problems are outlined.

ACKNOWLEDGMENTS

I thank the Matsumae International Foundation under whose Fellowship the main part of this work was carried out. I am delighted to acknowledge Professor H. Daiguji, at the Tohoku University in Sendai, for his invaluable support and the provision of computer facilities during the Fellowship. Finally, I thank Professor L. Roeva at the Bakulev Institute of Cardiovascular Surgery in Moscow, for attracting my attention to the problem discussed in this paper.

REFERENCES

1. C. Begue, C. Conca, F. Murat, and O. Pironneau. Les équationes de Stokes et de Navier–Stokes avec des conditions aux limites sur la pression, in *Nonlinear Partial Differential Equations and Their Applications: Collège de France Seminar,* edited by H. Brezis and J. L. Lions, Vol. IX (Longman, 1988), p. 179. [French]
2. C. G. Caro, T. J. Pedley, R. C. Schroter, and W. A. Seed, *The Mechanics of the Circulation* (Oxford Univ. Press, Oxford, 1978).
3. G. Chesshire and W. D. Henshaw, Composite overlapping meshes for the solution of partial differential equations. *J. Comput. Phys.* **90**(1), 1 (1990).
4. A. Chorin, A numerical method for solving incompressible viscous flow problems, *J. Comput. Phys.*, **2**(1), 12 (1967).
5. M. R. de Leval, P. Kilner, M. Gewillig, and C. Bull, Total cavopulmonary connection: A logical alternative to atriopulmonary connection for complex Fontan operations, *J. Thoracic Cardiovascular Surgery* **96**(5), 682 (1988).
6. G. E. Forsythe and C. B. Moler, *Computer Solution of Linear Algebraic Systems* (Prentice-Hall, Englewood Cliffs, NJ, 1967).
7. R. Hunt, The numerical solution of the flow in a general bifurcating channel at moderately high Reynolds number using boundary-fitted co-ordinates, primitive variables and Newton iteration, *Int. J. Numer. Methods Fluids* **17,** 711 (1993).
8. I. E. Idelchik, *Handbook of Hydraulic Resistance,* (CRC, Boca Raton, 1994).
9. R. W. Jeppson, *Analysis of Flow in Pipe Networks,* Ann Arbor Science, Ann Arbor, MI, 1983.
10. C. Kiris, S. E. Rogers, D. Kwak, and I. D. Chang, Computation of incompressible viscous flows through artificial heart devices with moving boundaries, in *Fluid Dynamics in Biology: Proceedings of an AMS-IMS-SIAM Joint Research Conference,* edited by A. Y. Cheer and C. P. van Dam, *1991,* p. 237.
11. H. T. Low, Y. T. Chew, and C. N. Lee, Flow studies on atriopulmonary connections of the Fontan operations for congenital heart defects, *J. Biomed. Eng.* **15**(4), 303 (1993).
12. Y. P. Marx, Evaluation of the artificial compressibility method for the solution of the incompressible Navier–Stokes equations, in *Proceedings, Ninth GAMM-Conference on Numerical Methods in Fluid Mechanics,* Vol. 35, edited by J. B. Vos, A. Rizzi, and I. L. Ryhming, (Vieweg, Braunschweig/Wiesbaden, 1992), p. 201.
13. Y. P. Marx, Time integration schemes for the unsteady incompressible Navier–Stokes equations, *J. Comput. Phys.* **112**(1), 182 (1994).
14. C. S. Peskin, The immersed boundary method for biological fluid dynamics, in *ICIAM 95. Programm, Hamburg, 1995, GAMM,* p. 86.
15. V. P. Podzolkov, M. R. Chiaureli, S. B. Zaets, I. A. Yurlov, L. M. Zotova, and I. A. Nekrasova, Total cavopulmonary anastomosis in surgery of complicated congenital heart anomalies, *Grudnaya Khirurgiya* **6,** 11 (1990). [Russian]
16. S. E. Rogers, A comparison of implicit schemes for the incompressible Navier–Stokes equations with artificial compressibility, *AIAA J.* **33**(11), 2066 (1995).
17. S. E. Rogers, D. Kwak, and C. Kiris, Paper 89-0463, AIAA, 1989 (unpublished).
18. D. A. Steinman, B. Vinh, C. R. Ethier, M. Ojha, R. S. C. Cobbold, and K. W. Johnston, A numerical simulation of flow in a two-dimensional end-to-side anastomosis model, *Trans. ASME J. Biomech. Eng.* **115**(1), 112 (1993).
19. V. K. Sud, R. S. Srinivasan, J. B. Charles, and M. W. Bungo, Mathematical modelling of the human cardiovascular system, *Phys. Med. & Biol.* **38**(3), 369 (1993).
20. E. Turkel, Preconditioned methods for solving the incompressible and low speed compressible equations, *J. Comput. Phys.* **72**(2), 277 (1987).
21. S. Yamamoto and H. Daiguji, Higher-order-accurate upwind schemes for solving the compressible Euler and Navier–Stokes equations, *Comput. & Fluids* **22**(2/3), 259 (1993).